

A Comparative Analysis of Low-Aspect-Ratio Conventional and Single Slotted Circulation Control Foils Intended for Marine Hydrodynamic Applications

AUTHORS

Samuel M. Granger
62 Cedar St #311, Seattle WA, 98121
(860) 985-1633 – grangersam@gmail.com

Randall P. Neureuter
2400 4th Ave #335, Seattle WA, 98121
(716) 341-1295 – rneureuter@gmail.com

ADVISOR

Richard Royce
Webb Institute
298 Crescent Beach Rd
Glen Cove NY, 11542
webb.edu

A Comparative Analysis of Low-Aspect-Ratio Conventional and Single-Slotted Circulation Control Foils Intended for Marine Hydrodynamic Applications

ABSTRACT

Lifting surfaces are used in various marine applications that require high lift generation with minimal drag. This thesis investigates the application of circulation control (CC) on a submerged wing using the circulating water channel in Haerberle Laboratory at Webb Institute. The objective of this thesis is to design and construct a CC foil within established parameters from previous work and to determine the increase in lift and analyze three-dimensional effects on the CC foil compared with a conventional foil. Two model foils were developed. The first is a conventional NACA 65-015 foil, and the second is the same section with a modified CC trailing edge. The lift and drag forces developed by each foil were compared for testing with and without endplates. Moderate blowing from the CC slot at zero angle of attack exceeded the lift force generated by the conventional foil throughout the test matrix. As expected, endplate testing yielded an increase in lift, but further improvement could be made by using a larger endplate to further mitigate tip vortices.

NOMENCLATURE

α	Angle of attack
AR	Aspect ratio
AR_e	Effective aspect ratio
c	Foil chord length
C_D	Drag coefficient
C_L	Lift coefficient
C_P	Pressure coefficient
C_μ	Momentum coefficient
D	Drag
D'	Drag per unit span
g	Acceleration due to gravity
h	Slot height
L	Lift
L'	Lift per unit span
m_j	Jet mass flow rate

p	Fluid pressure
q	Dynamic pressure
r	Trailing edge Coanda radius
S	Wetted surface area
t	Foil maximum thickness
V_∞	Free stream velocity
V_j	Jet velocity
α	Geometric angle of attack
Γ	Circulation
ρ	Fluid density

INTRODUCTION

In the design of lifting surfaces, there is a constant effort to enhance performance. The aerospace industry developed an active technique known as circulation control (CC), which offers dramatically increased lift. CC uses a high-velocity-fluid jet that follows a modified, rounded trailing edge to alter the pressure distribution of the wing. Heavy-lift aircraft employ this technique at low speed for short take-off and landing (STOL) purposes. There is interest in marine applications of this technology for rudders, propeller ducts, autonomous underwater vehicle (AUV) control surfaces, and submarine stern planes. Currently, there is no marine full-scale application of this technology, despite its potential to create significantly more effective lifting surfaces for vessel control applications.

The intention of this thesis was to advance the study of CC wings for marine hydrodynamic applications. The primary objective of this thesis was to determine the increase in lift of a CC foil compared to a conventional foil. This was accomplished by testing two models, a conventional foil and a CC foil, using the flow channel in Haerberle Lab at Webb Institute. The secondary objective of this thesis was to analyze three-dimensional effects of a low-aspect-ratio CC wing.

The first part of this paper explores the previous work related to CC technology in the aerospace industry and the past research performed for marine applications. The following section discusses the theory of conventional wing sections and CC wing sections, using both two-dimensional and three-dimensional approaches. The next section touches on the procedure for the design, construction, and testing of a conventional and CC wing. This discussion is followed by a review of the results, conclusions, and recommendations for future work.

BACKGROUND

CIRCULATION CONTROL

Circulation control is an active lift augmentation method that can be applied to a variety of fluid dynamic systems (Kweder 2012). Research and development of this technology has been ongoing since the 1960s. The focus of this research was fixed-wing aircraft with trailing-edge blowing. In this application, high-velocity fluid is injected into the flow around the wing. The injected flow on the low-pressure side of the wing keeps the flow attached to the surface of the wing around a rounded trailing edge. The attached flow around the trailing edge, known as the Coanda effect, delays boundary layer separation and increases circulation around the foil. Figure 1 shows the tangential fluid ejection out of a duct through a slot. The high-velocity fluid remains attached to the surface until a point of separation on the high pressure side of the foil. An in-depth analysis of CC theory is presented later in this paper.

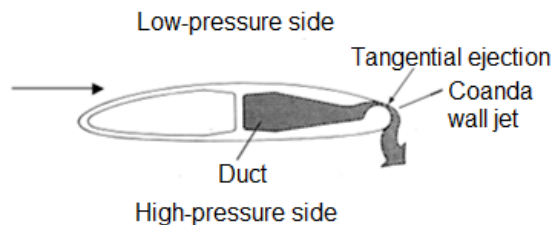


Figure 1. CC Trailing Edge
Source: Rogers, 2004

AERONAUTICAL APPLICATIONS

CC is currently being used in applications where heavy lift is required. It is applied to increase the capacity of an aircraft, increase passenger comfort at low speeds, and/or increase aircraft capabilities by

decreasing their takeoff and landing requirements. The US Air Force, NASA, and Boeing completed extensive research into the application resulting in prototypes for STOL aircraft, no tail rotor (NOTAR) helicopters, and the C-17 Globemaster.

The STOL aircraft concepts use exhaust gases ejected above the wing to increase lift, resulting in lower takeoff and landing speeds. Therefore, take-offs and landings can be achieved on shorter runways. Figure 2 is an image of the U.S. Navy STOL concept.



Figure 2. US Navy/NASA Super-STOL Concept
Source: Englar, 2004

For helicopter uses, *NOTAR* was developed in order to provide the thrust required for stable helicopter flight without a tail rotor. This system uses CC acting along the length of the tail boom to produce the required horizontal force to keep the helicopter stable. A fan blows ambient air into the tail boom for CC. CC is sufficient only for stable flight; a jet thruster is necessary for sufficient maneuverability (Ward, 7). The NOTAR system is shown in Figure 3.

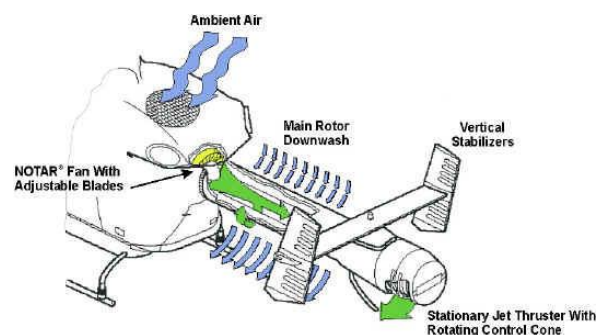


Figure 3. NOTAR System
Source: MD Helicopters, 2013

The C-17 Globemaster III uses slotted flaps that are lowered into the exhaust stream in order to increase

lift and decrease the minimum controllable airspeed, allowing for lower angles of attack on descent and reduced airstrip lengths.

A study done by Kweder, *et al.* at West Virginia University showed that a respectable gain can be achieved by applying a passive circulation system to the propeller of a fixed-wing aircraft. For aircraft, any additional weight, such as the weight required to run an active circulation control system, comes with a major cost. This cost makes active CC, where air is moved by a blower, very difficult to justify. In order to decrease weight, the study examined a passive system where the jet of blown air on the trailing edge of the propeller is developed from the stagnation pressure on the leading edge of the blade. By reducing the weight that is required to run the system, a modest gain of 6% efficiency was realized with little impact. This gain persisted over the entire operating range of the propeller, including the crucial loading conditions during take-off and landing. Kweder, *et al.* built on the findings of a NASA sponsored study in 1981, which found that there could be a 7% decrease in fuel usage in cruising conditions by applying active circulation control to a propeller. The NASA study, however, did not take into account the penalties that are associated with additional weight and complexity in construction, operation, and maintenance. These additional difficulties currently make an active circulation system on an aircraft propeller unfeasible.

MARINE APPLICATIONS

The focus of hydrodynamic research into CC has been to augment lift of control surfaces. Wind tunnels and model basins have been utilized for the testing of such devices; however, a full-scale test of such a device has yet to be completed.

Research on lift generation on submarine stern plates in 1971 demonstrated that there is a considerable performance increase that can be achieved by applying CC. This was accomplished by changing from four movable-flap control planes to four fixed, elliptical, dual-slotted CC planes. Further hydrodynamic research showed a potential performance increase that may be achieved by modernizing the foil shape (Englar).

Little research on marine applications of CC was published between 1971 and 1996, until Zhu tested a high-lift CC rudder at the University of North Carolina. A NACA 0015 foil section was chosen for the model. The trailing edge was modified with a rounded Coanda surface. Zhu found that the lift augmentation for a low-aspect-ratio rudder is much lower than the expected augmentation from a two-dimensional CC rudder. There is significant jet momentum loss in the three-dimensional model, which negatively effects the lift augmentation. Endplates were fixed to both ends of the rudder model, as shown in Figure 4, to reduce those effects.

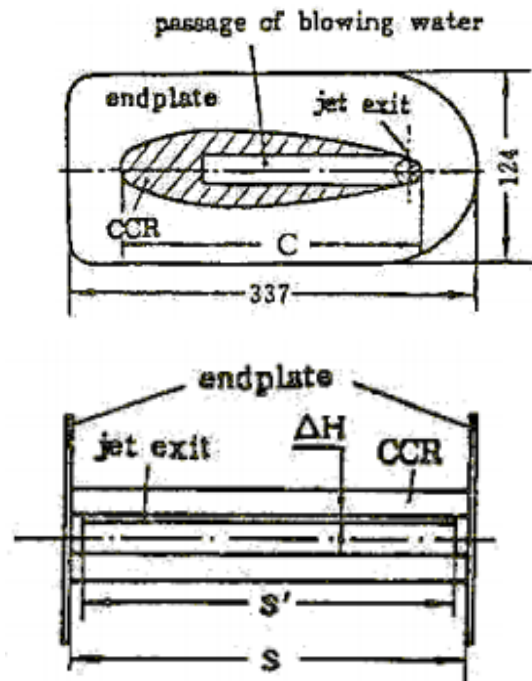


Figure 4. Single-Slot CC Rudder
Source: Zhu, 1996

In 2000, N.A. Brown tested the maneuvering capabilities of a CC propeller duct at the University of New Orleans. In that research, Brown analyzed the effectiveness of introducing CC in order to increase maneuverability at low speed and potentially replacing hydraulically actuated control surfaces with fixed CC surfaces. The research discovered a large increase in lift from a Kort-nozzle propulsor in low-speed maneuvering, but poor performance in the bollard condition.

Brown's findings were confirmed by Ward (2006) in a study at the University of Glasgow. Ward used a theoretical approach to study the effect of fitting a CC propeller duct to a US Navy AUV. The CC system used in Ward's research is designed so that the lift at six knots, the AUV's top speed, matches that of the conventional rudder lift. Ward's research determined that at low speed an increase of six times the maneuvering force is possible with a ducted propeller using CC. At higher speed this benefit was shown to decrease, but at no time was the maneuvering force less with the CC duct than with the original rudder. However, lift could have been further improved by increasing the fluid flow from the slot. The research further shows that an increase of 9.5% in efficiency can be realized as a result of decreased drag from foil deflection. The report also analyzed the power consumption from the pump required for maneuvering. It determined that in order to achieve the maximum maneuvering force of 700N that the AUV originally had been capable of at a speed of six knots, a pump output power of 70 watts was required.

A paper published by Rogers and Donnelly (2004) investigated a low-aspect-ratio hydrofoil with dual blowing. An upper and lower slot, as shown on the left of the model in Figure 5, were used to achieve dual blowing. Dual-slot blowing improves performance at higher jet velocities, V_j . The benefit from dual slot blowing is more difficult to achieve as it requires two separate ducts with different fluid flow rates.

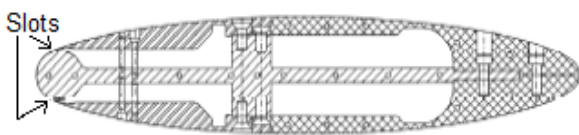


Figure 5. Dual Blowing Model Cross Section
Source: Rogers, 2004

THEORY

HYDRODYNAMIC FOIL SECTION DESIGN

Hydrodynamic section design uses an analytical approach to achieve desired characteristics for lift and drag at different operating points defined by angle of attack and fluid velocity. The lift force a section can generate originates from a velocity-induced pressure profile around the section. Altering the pressure

profile modifies the characteristics of a section. Optimal section design of lifting surfaces such as aircraft wings typically involves a required lift force necessary for flight and a desire to minimize drag. In designing other sections, such as a ship's rudder, it is also advantageous to maximize lift generation at a variety of angles while also minimizing drag.

The majority of foil section designs originate from extensive research conducted by the National Advisory Committee for Aeronautics (NACA) in the 1930s. NACA developed airfoil series from analytical equations that describe the camber of the mean-line of the section as well as the thickness distribution along the length of the section (Anderson). These sections are the four-digit and five-digit NACA series. Later, NACA developed the NACA 6-series using theoretical methods.

In order to discuss further the theory of section design, several terms must be defined. The chord c is the length between the leading and trailing edge of a section. The maximum thickness of a section t is measured perpendicular to the chord. The planform area of a rectangular wing S is the chord length multiplied by the span b . Figure 6 shows a NACA foil section with camber. Similarly, a symmetric section has no camber, so that the mean camber line is coincident with the chord line and the foil is mirrored across its chord line.

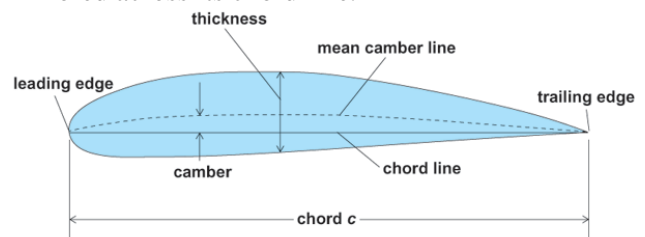


Figure 6. NACA Airfoil Section
Source: Anderson, 2014

TWO-DIMENSIONAL FOIL CHARACTERISTICS

Conventional Sections

Abbott and von Doenhoff provide foil characteristics along with the two- and three-dimensional foil theory for initial analysis. Their two-dimensional analysis expresses lift and drag in terms of force-per-unit-span. Lift is defined as the component of force acting in a direction perpendicular to the line of flight; drag

is the force directly opposing the motion of the wing. Lift- and drag-per-unit-span are given by

$$L' = \frac{1}{2} C_L \rho V_\infty^2 c, \quad (1)$$

and

$$D' = \frac{1}{2} C_D \rho V_\infty^2 c. \quad (2)$$

Potential flow theory can be used to analyze the flow around a conventional foil section, where the Kutta condition must be applied to obtain a physical solution. This condition requires that the rear stagnation point be located at the trailing edge of the section in a steady flow. Without specifying the Kutta condition, the solution will be unphysical, as the flow over the lower surface, the pressure side of the foil, must pass around the trailing edge with a near infinite velocity to connect to the flow over the upper surface. This unphysical event results in a solution with zero lift and zero drag. The Kutta condition requires the fluid velocity to be finite. For the condition to be satisfied, the foil section must develop sufficient circulation Γ to move the stagnation point to the trailing edge. The circulation adds to the uniform flow on the low-pressure side of the wing and subtracts from it on the high-pressure side, resulting in greater fluid velocity on the low-pressure surface of the foil than on the high-pressure surface. A velocity-induced pressure gradient is produced around the section. The Kutta-Joukowski theorem is used to calculate the lift-per-unit-length L' generated by a foil section where,

$$L' = -\rho V_\infty \Gamma. \quad (3)$$

Circulation Control Sections

It is evident from conventional, two-dimensional wing theory that the lift resulting from flow over a surface is influenced strongly by the boundary condition at the trailing edge. For conventional sections this is defined by the Kutta condition in potential flow. As previously mentioned, CC is a technique that effectively moves the trailing edge stagnation point around a rounded trailing edge surface to the high pressure side. Altering the location of the separation of flow from the trailing edge will significantly affect the lift developed by a section. Figure 7 illustrates the differences between a conventional and a CC trailing edge. High pressure fluid is ejected tangential to the flow over the section. The ejected fluid jet becomes entrained in the upstream surface flow. The resulting fluid jet remains

attached to the curved surface. The Coanda effect is simply the tendency of this fluid jet to be attached to a nearby surface. The absence of a sharp trailing edge removes the constraint of the Kutta condition, allowing the circulation to be freely influenced by active control (Rogers and Donnelly 2004).

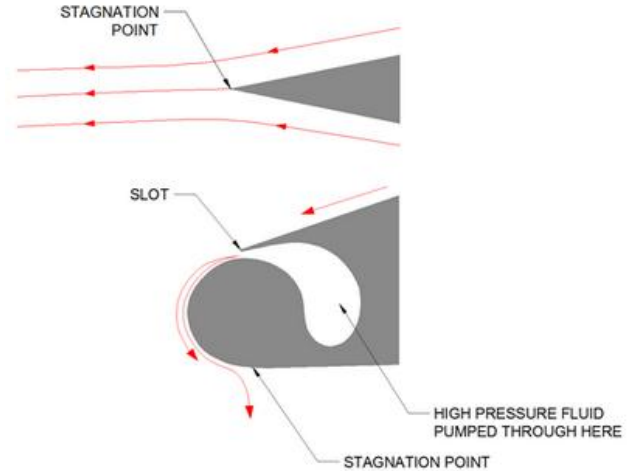


Figure 7. Trailing Edge Comparison

CC performance generally is analyzed using the slot-flow momentum coefficient C_μ . The momentum coefficient is the ratio of jet momentum to the product of the free-stream dynamic pressure and the surface area. Assuming incompressible flow, the momentum coefficient is defined as

$$C_\mu = \frac{m_j V_j}{qA}, \quad (4)$$

or

$$C_\mu = 2 \frac{h}{c} \left(\frac{V_j}{V_\infty} \right)^2, \quad (5)$$

where m_j is the mass flow rate of water from the slot, q is the dynamic pressure, A is the area, h/c is the height-to-chord-length ratio, and V_j/V_∞ is the velocity ratio. The typical range of C_μ is from 0.0 to roughly 0.2 (Rogers and Donnelly 2004). Above a momentum coefficient of 0.3 excessive jet turning will occur. Methods of overcoming excess jet turning include dual-slot blowing or the use of a small secondary diameter at the trailing edge. Both methods force the flow to detach at a designed location along the rounded trailing edge.

A square-root relationship exists between the momentum coefficient C_μ and the lift coefficient C_L . This relationship is reported by the authors Englar,

Rogers, and Zhu. Ward fit curves to the experimental data presented by these other authors in his paper and develops the following equations for lift and drag,

$$C_L = 10\sqrt{C_{\mu}}, \quad (6)$$

and

$$C_D = 13C_{\mu}. \quad (7)$$

These equations can be used along with Eqs. 1 and 2 to determine the lift- and drag-per-unit-span produced by a CC section.

Figure 8 is a representative pressure distribution for a CC foil compared to that of a conventional foil section. The pressure distribution for the leading edge section remains unchanged. An obvious change in the pressure distribution for the trailing half of the section is present with a sharp drop in pressure around the trailing edge. This is the area of low pressure emanating from the fluid jet ejected over the Coanda radius.

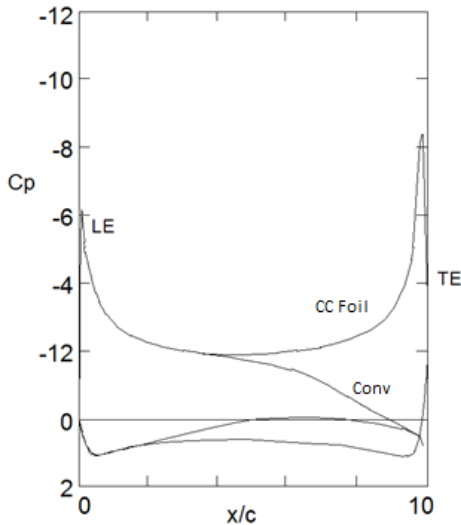


Figure 8. Comparison of Pressure Distribution for CC and Conventional Foils
Adapted from: Rogers, 2004

THREE-DIMENSIONAL FOIL FLOW CHARACTERISTICS

Real wings are not infinitely long, as are those modeled in the two-dimensional case. The three-dimensional case must incorporate finite span with a free end. Because the pressure is higher on one side of the foil, flow naturally tends to move around the tip to the low-pressure side. A downward motion of the flow is created, that increases with closer proximity to the wingtip, as illustrated in Figure 9. A

corresponding upward motion is created on the opposing side of the wing. Because the directions of flow over each side of the foil are different, when the two flows meet at the trailing edge, vortices are created. The resulting vortices change the flow in the wake region, deflecting downward opposite to the direction of lift. These vortices are particularly strong at the wingtip.

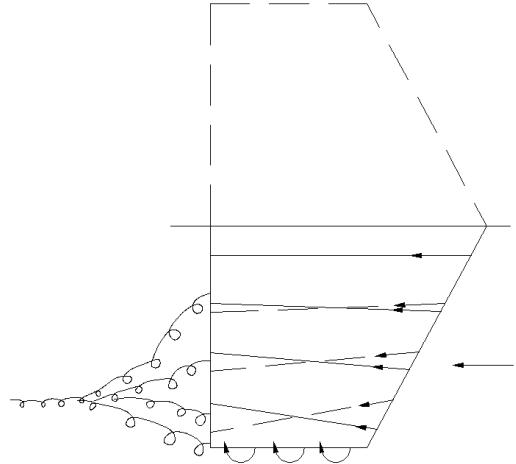


Figure 9. Flow over a 3D Wing
Source: Larsson, 2007

Prandtl lifting-line theory is used to compute the lift distribution over a three-dimensional wing. In Prandtl's theory, trailing vortices from the wing tips are connected by a bound vortex. The bound vortex generates the circulation that produces the lift (Munson, Young and Okiishi, 546). The combined vortex system, shown in Figure 10, is called a horseshoe vortex. Figure 11 is a simplified illustration of the leakage around the wing tips that produces the trailing vortices. The strength of the trailing vortices is equal to the strength of the bound vortex and proportional to the lift generated. The total lift for a foil is calculated from

$$L_{total} = \rho V_{\infty} \int_{tip}^{tip} \Gamma(y) dy, \quad (8)$$

where the circulation is the strength of the bound vortex at a point along the span. Two useful approximations for the initial analysis of finite length wings are Prandtl's formula,

$$C_L = \frac{C_{L,2D}}{1 + \frac{2}{AR}} \alpha, \quad (9)$$

and Helmbold's formula,

$$C_L = \frac{C_{L,2D}}{\sqrt{1 + \left(\frac{2}{AR}\right)^2 + \frac{2}{AR}}} \alpha, \quad (10)$$

where $C_{L,2D}$ is the two-dimensional lift coefficient. AR is the aspect ratio, defined as the span b divided by the chord length c . α is the angle of attack. Equation 9 is for wings with for which $AR > 4$, while Equation 10 is applicable to wings having $AR < 4$. Based on these two equations, it is evident that aspect ratio has a significant effect on the lift generated by a three-dimensional wing. This is evident in the decreasing slope of the lift coefficient curve at varying angles of attack in Figure 12 as the aspect ratio decreases.

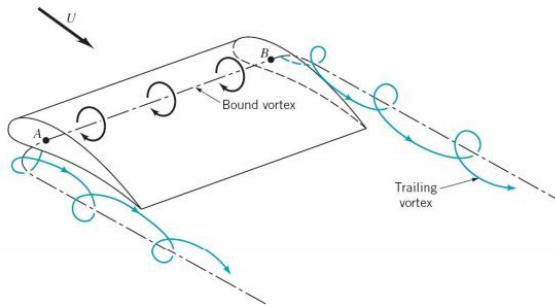


Figure 10. Wing Vortex System
Source: Munson, 2006

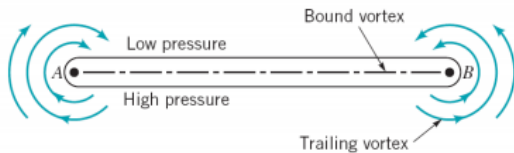


Figure 11. Front View of Wing Vortex System
Source: Munson, 2006

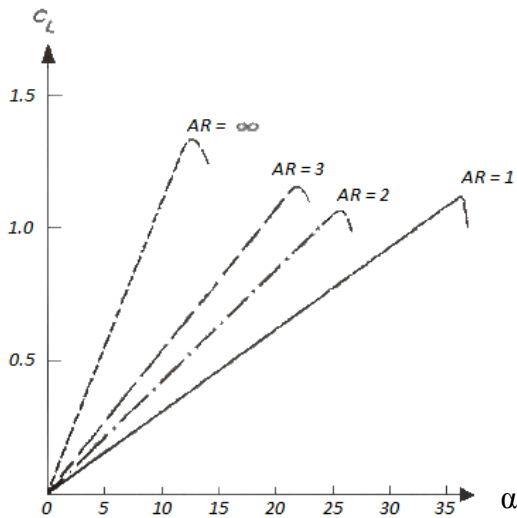


Figure 12. Influence of Aspect Ratio on Lift
Source: Larsson & Eliasson, 2007

PROCEDURE

FOIL DESIGN

Foil Selection

The foil section was selected based on the original objective of this thesis, which was to develop a CC sailing yacht keel to test in the Robinson Model Basin. Larsson and Eliasson’s *Principles of Yacht Design* (2007) recommends the use of 63- or 65-series NACA foils with a thickness of 12 to 18%. NACA 63- and 65-series sections are known as laminar foils because of their large region of laminar flow, which is the result of a minimum pressure peak close to the trailing edge. The larger laminar region results in improved lift and drag performance at low angles of attack but also earlier stall. These foils are optimal for the conditions seen during sailing because the angle of attack of the keel is generally only two to four degrees. Figure 13 shows the drag characteristics for a NACA 65-015 foil section. Notice the significant decrease in the drag coefficient at small values of lift coefficient. These low lift coefficients correspond to low angles of attack, and the 63- and 65-series are said to operate in a region known as the “drag bucket” giving them excellent drag characteristics for keels.

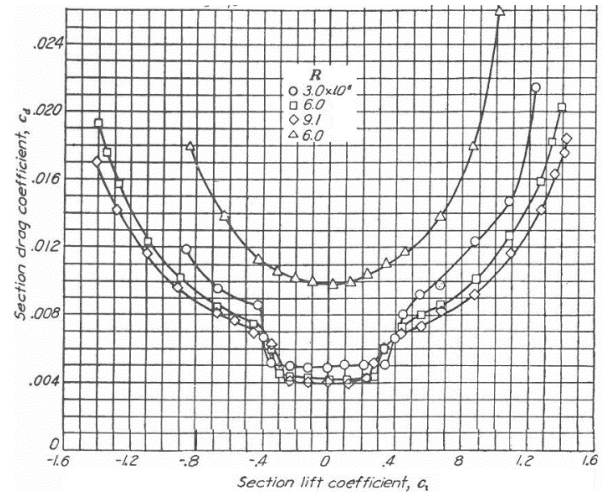


Figure 13. NACA 65-015 Drag Characteristics
Source: Adapted from Abbott, 1949

An analysis was performed using the program XFLR5 to determine the appropriate thickness-to-chord-length ratio for operational angles of attack of a typical keel. The lift-to-drag ratio for the NACA 65-series is shown in Figure 14 for thickness-to-

chord-length ratios of 12% to 18%. It was determined that the NACA 65-012 offered the best lift and drag characteristics; however, this was not the only criterion for selecting an appropriate thickness. The model also had to be sufficiently thick to withstand the forces anticipated during testing. The foil was modeled as a simple cantilever beam with a distributed load generated by the lift and drag forces predicted in the XFLR5 analysis. After this analysis, it was determined that a slightly thicker foil would be beneficial to minimize the forces at the point where the foil was mounted to the apparatus. A NACA 65-015 section (Figure 15) was the final selection based on both the XFLR5 and stress analyses.

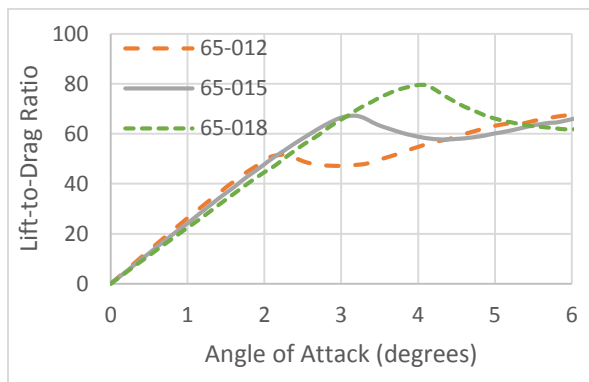


Figure 14. XFLR5 Analysis for NACA 65-Series

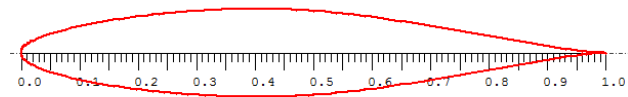


Figure 15. NACA 65-015 Foil Section

CC Foil Design

Prior testing has shown that the most effective trailing edge shape for circulation control is a circle. Table 1 shows a number of Coanda radius-to-chord-length ratios used in past studies. A Coanda radius of 5.4% was selected and is depicted in the Figure 16. Past studies show that a Coanda radius-to-chord-length ratio between 2% and 5% yields good attachment of flow around the trailing edge (Englar and Williams, 17). A radius outside this range was chosen in order to limit the size of the foil, decreasing both the manufacturing cost and the forces developed. The slot-height-to-chord-length ratio was determined from past experimentation to be most effective between 0.10% and 0.25%, and 0.25% was chosen. Figure 17 is a plot showing the most effective

operating region for a circulation control trailing edge. The dimensions chosen for this design fall at the indicated point at the upper right-hand corner of this region to limit the overall dimensions of the foil and thus reduce the fabrication cost.

Table 1. Previous Coanda Radius-to-Chord-Length Ratios
Source: Adapted from Ward, 2006

Author	Model	r/c
Englar (1971)	Submarine stern plane	0.0384
Zhu and Xianfu	Rudder	0.0253
Rogers (2004)	Naval hydrodynamic applications	0.0428
Englar (2004)	STOL aircraft	0.0429
Ward	Large diameter propeller duct	0.0429
	Small diameter propeller duct	0.0200

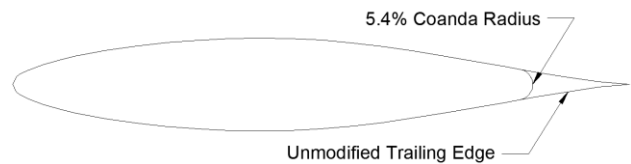


Figure 16. NACA 65-015 Modified Trailing Edge

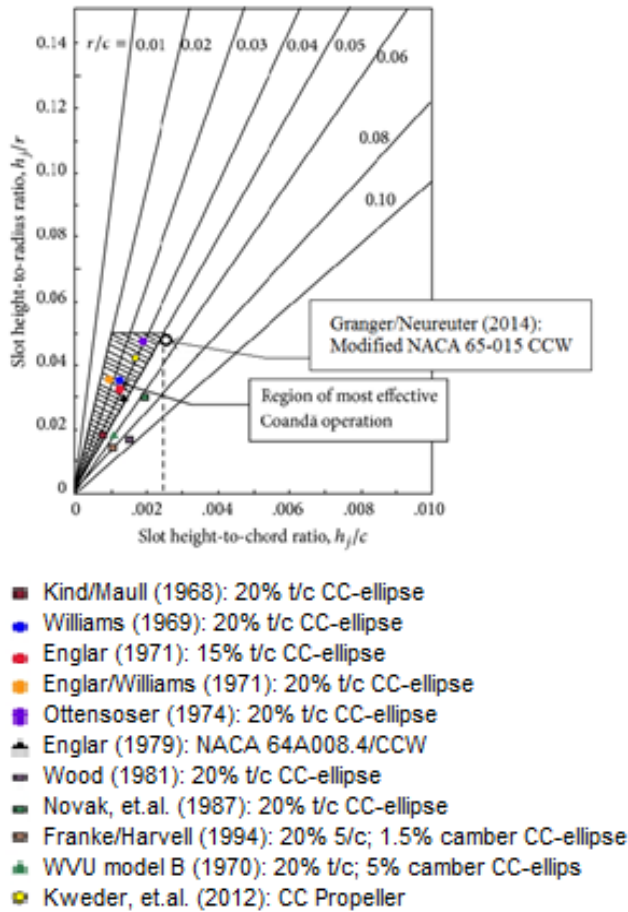


Figure 17. Most Effective Circulation Control Geometry
Adapted from: Kweder, et al., 2012

The sizes of both foils were driven by the manufacturing capabilities for the trailing edge of the CC foil. Tolerance limitations from of the type of three-dimensional printing used, stereolithography, required the slot height to be a minimum of 0.040 inches. Using the design criteria of a slot-height-to-chord ratio of 0.25% and a Coanda radius-to-chord-length ratio of 5.4%, it was determined that the CC foil should have a chord length of 16 inches and a radius of 0.83 inches. The chord length of the conventional foil is 20.47 inches. A span of 12 inches was chosen in order to limit the cost of fabrication, limit the lift forces and keep the AR low.

A plenum running the span of the foil incorporated a slot that allowed fluid to be ejected around the radius. A plan view of the trailing edge section of foil at its root is shown in Figure 18.

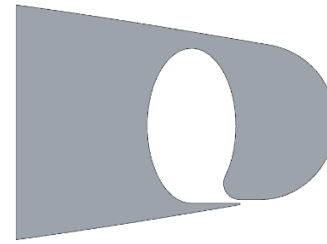


Figure 18. Root Plenum Plan View

The plenum is tapered along the span of the foil to ensure that gauge pressure remains constant along the slot. The amount of taper was calculated using Bernoulli's equation,

$$\frac{v^2}{2} + gz + \frac{p}{\rho} = \text{constant}, \quad (11)$$

to account for viscous losses. By keeping the velocity in the plenum constant, the slot pressure varied only with water depth, identical to the pressure outside of the foil. Figure 19 shows two renderings of the final trailing edge model. Figure 19a shows the circular fluid inlet at the top of the trailing edge, which was connected to the piping system, and the slot located at the start of the Coanda radius. Figure 19b is a view of the inside of the same section showing the tapered plenum that feeds the slot.

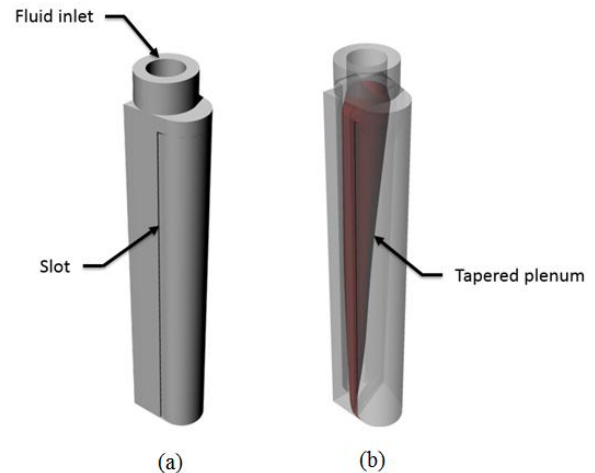


Figure 19. Renderings of Stereolithography Trailing Edge

CC Foil Modification Effects

In order to accommodate the circular trailing edge, the trailing edge of the conventional foil was trimmed to maintain the radius tangent to the foil. Because the thickness distribution of the original NACA 65-015

foil section remains unchanged, the decreased chord length changes the relative position and relative magnitude of the maximum thickness. As a result of the decreased chord length, the maximum foil thickness increased from 15.0% to 19.4% of the chord length. The location of the maximum thickness also moved back from 40.7% to 52.8% of the chord length; however, the distances were held constant.

An analysis was performed using XFLR5 to determine the consequences that the changes have on the conventional foil's lift and drag characteristics. This analysis gives an accurate prediction of the characteristics of the CC foil section. Without this comparison, a third foil would have been required to show that the changing of the thickness and thickness distribution was not the cause of the changes in lift experienced by the CC foil relative to the conventional foil. The third foil would effectively have been a modified NACA 65-019 with the maximum thickness at 52.8% chord, giving it the same principal dimensions as the CC foil, but with a conventional trailing edge. Figure 20 and Figure 21 show the effect of the changes made to the original NACA section.

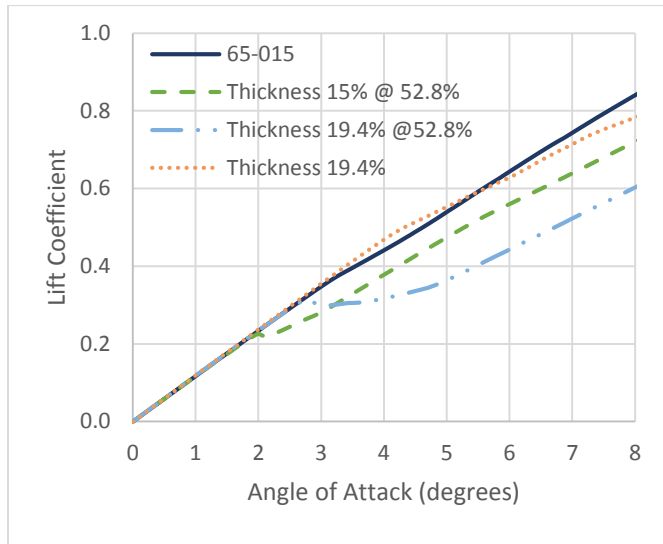


Figure 20. Third Foil Lift Coefficient Comparison

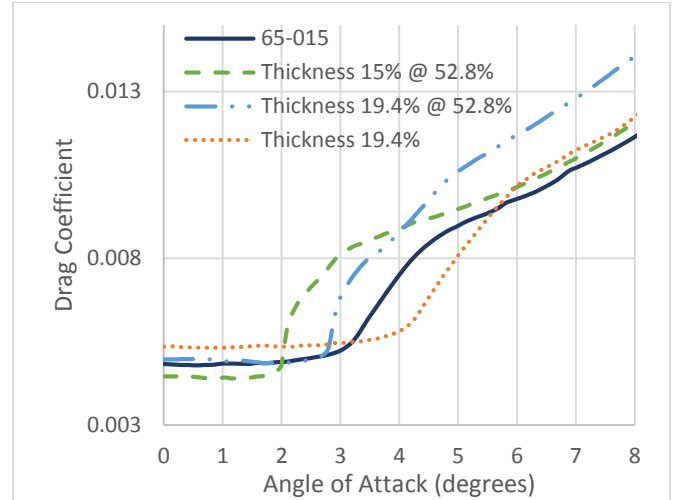


Figure 21. Third Foil Drag Coefficient Comparison

At all angles of attack the modified foil section with 19.4% thickness at 52.8% chord was calculated to provide less or equal lift with greater or equal drag compared to the unmodified foil. This analysis showed that it was unnecessary to compare a third physical foil, as that foil would have less desirable performance than the unmodified foil, meaning that any positive changes to the performance of the CC foil were not due to the geometric modifications.

MODEL CONSTRUCTION

Webb Institute's CNC model cutter was used to create the entire conventional foil and the leading portion of the CC foil. The foils were designed in Rhinoceros 5.0 and loaded into PartWorks 3D, which generated the tool paths used by the cutter. The foils were split down their mean camber lines and the two halves were cut from two-inch-thick, high-density model foam, as shown in Figure 22.

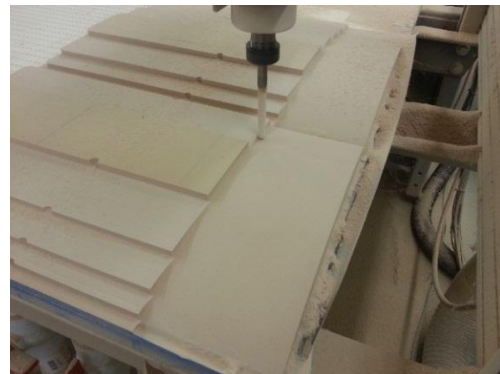


Figure 22. Foil Cutting

The model cutting was done in three steps. First, the side coincident with the mean camber line was surfaced to ensure that it was flat, and alignment holes were drilled for use during final assembly. Next, a rough cut was made of the foil shape, leaving the steps in the foam that are visible in Figure 22. Finally, the foil shape was cut. In order to decrease cutting time, a relatively large ball end mill was used for the final cut, which necessitated subsequent sanding by hand to achieve a sufficiently smooth surface. Layers of epoxy and paint were applied to the foam as waterproofing. After having been epoxied and painted, the foils were sanded again until it was smooth.

APPARATUS

The testing apparatus was designed to allow measurement of lift and drag forces of the CC and conventional foils at various angles of attack in the Haeberle Laboratory flow channel. In order to accomplish this, the apparatus was fitted with two force blocks, one in line with the flow and the other perpendicular to the flow. A rendering of the apparatus with the conventional foil is shown in Figure 23. The force blocks, shown in red, were situated such that they were as close to the foils as possible while remaining above the still water line of the flow channel. This was done to minimize the moments applied to the force blocks while still ensuring that there was no possibility of the blocks becoming submerged.

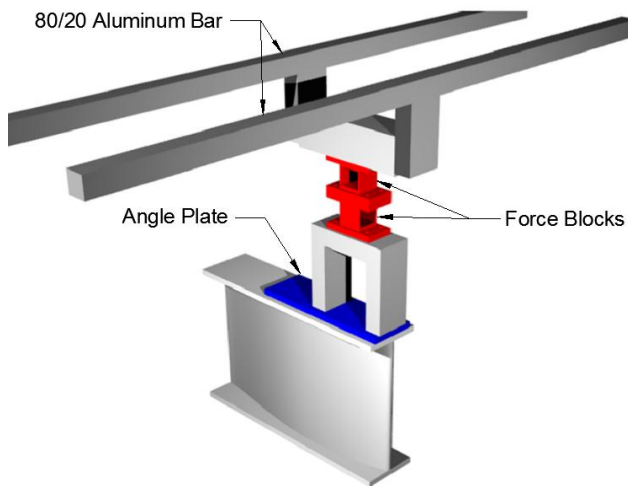


Figure 23. Apparatus with Conventional Foil and Endplates

The foils were held at fixed angles using the angle plate, shown in blue in Figure 23, which has bolt holes that correspond to holes in the top of the foils. This arrangement allows the foils to be fixed at each angle of attack under test. Two bolts, one that determined the angle and the other that acted as the center of rotation, fixed the foil to the apparatus. The structure of the apparatus was made of 80/20 extruded aluminum bar. The plates for the foil endplates, force block mounts, and angle of attack were ½ inch PVC.

The plumbing system for the CC foil consisted of a pump, flow meter, and globe valve, all connected using ¾ inch PVC pipe. Two Hydronix inline-type flow meters were used in order to measure the range of flow rates in the test matrix. The centrifugal pump, which is capable of a maximum flow rate of 21 gallons per minute, drew water directly from the flow channel. The flow was regulated using a globe valve.

FLOW CHANNEL

The flow channel (Figure 24), designed by Edinburgh Designs, was installed in Haeberle Laboratory in January of 2012. It uses a variable-speed 60-hp motor to drive an impeller that can produce flow speeds of up to nine feet per second. The flow speed is set by the frequency at which the motor operates. Because the controls do not directly control the flow channel speed, a Pitot tube downstream of the foil and situated in undisturbed flow was used to determine the speed. The Pitot tube apparatus, shown in Figure 25, measures flow by measuring the static head that results from the flow's stagnation pressure. Before testing began, the flow-channel speeds developed at each motor frequency were determined.



Figure 24. Haeberle Laboratory Flow Channel



Figure 25. Pitot Tube

At higher speeds, the flow channel develops a standing wave in the test section. In order to mitigate the effects of this wave, the foils were tested away from the area where the wave developed and at a depth that submerged the top plate.

TEST MATRIX

Before testing of the model foils could begin, a test matrix was developed, shown in Table 2 and Table 3. Each test was run twice, once with and once without a bottom endplate. The angle of attack and flow channel speed were varied, as was the flow rate from the slot on the CC foil. Additionally, tests were run on the apparatus without a foil in order to determine the lift and drag forces that were not caused by the foil.

Table 2. Conventional Foil Test Matrix

α	V_∞								
0	0	2	0	4	0	6	0	8	0
	1		1		1		1		
	2		2		2		2		
	3		3		3		3		
	4		4		4		4		
	5		5		5		5		

Table 3. CC Foil Test Matrix

Angle of Attack, α									
0		2		4		6		8	
V_j/V_∞	V_∞	V_j/V_∞	V_∞	V_j/V_∞	V_∞	V_j/V_∞	V_∞	V_j/V_∞	V_∞
1	1	1	1	1	1	1	1	1	1
	2		2		2		2		
	3		3		3		3		
	4		4		4		4		
	5		5		5		5		
2	1	2	1	2	1	2	1	2	1
	2		2		2		2		
	3		3		3		3		
	4		4		4	4			
	5		5		5	5			
3	1	3	1	3	1	3	1	3	1
	2		2		2		2		
	3		3		3	3			
	4		4		4	4			
4	1	4	1	4	1	4	1	4	1
	2		2		2		2		
	3		3		3	3			

The test matrix was limited by a number of variables, including the force-block capacity and the water flow rate for the CC foil. The largest force blocks at Webb Institute are 20-pound and five pound capacity. For the CC foil, the water flow rate is limited by the flow that can be attained from the pump.

CALIBRATION

Prior to testing each day, it was necessary to calibrate the pair of force blocks. This was accomplished by applying known forces to the test apparatus below the force blocks. These forces were applied by suspending weights from the apparatus using a pulley system. The calibration trials were run for five seconds each at a flow rate of 0.0 ft/s. As a result of the applied force, the force blocks supplied a variable voltage signal to the Validyne equipment in the lab. LabView software was used to analyze the voltage inputs and determine averages. A linear regression was made of the recorded averages, and the

coefficient of determination of the regression was checked to ensure the precision of the measurements. The data output from the instrumentation is in volts, which, using the calibration data, is converted back into a force. Upon the completion of testing, a post-calibration was conducted in order to determine whether there had been any drift in the measurements and to ensure the validity of the data.

RESULTS

INITIAL PREDICTIONS

Initial analysis of the conventional foil was performed using XFLR5. Three-dimensional NACA 65-015 wing models for both infinite and finite ($AR_e = 1.16$) aspect ratios were defined.

The initial results for the CC foil in both cases are more challenging to obtain. At zero angle of attack, there are adequate data to suggest that lift has a square-root relationship with the momentum

coefficient, as suggested by theory. The plot in Figure 26 shows this relationship. The various points along the curve show the jet-velocity-to-channel-velocity ratio. The testing performed did not exceed a jet-to-channel velocity ratio of 4.0 which corresponds to a maximum lift coefficient of 2.83 at a momentum coefficient of 0.08. These values are for the infinite aspect ratio testing. The finite span testing became less predictable, but it is anticipated that the reduction in lift is similar to that of the conventional wing.

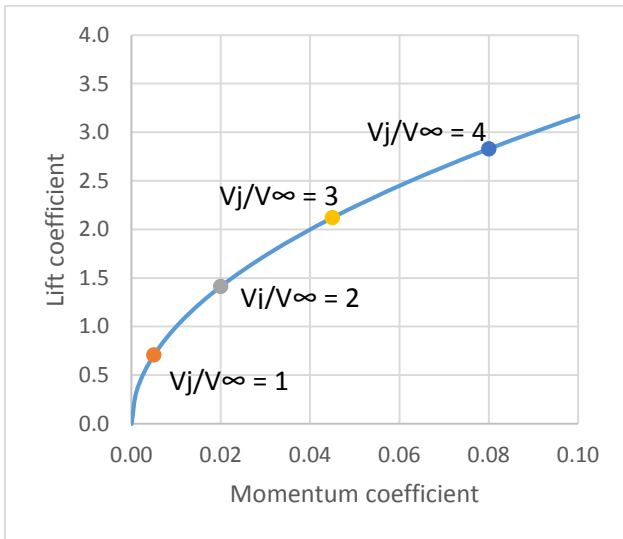


Figure 26. Relationship Between Lift Coefficient and Momentum Coefficient

Two approaches were used to predict the lift force for the CC wing at angles of attack other than zero. The first approach was numerical hand calculations, which superimposed the pressure distribution created by the fluid jet flow out of the slot over the trailing edge onto the pressure distribution of the parent conventional foil obtained from the XFLR5 analysis. This approach proved cumbersome and requires a number of assumptions to address unknowns regarding the superposition of flow. First, it is unknown if upstream flow will integrate fully with the flow exiting the slot. A second unknown is the location of the point of separation. This changes with varying model velocities, momentum coefficients, and angle of attack. Numerical integration methods were used to solve for the lift force generated by the combined flow.

The second approach is highly simplified. Generally, performance trends are predictable by imposing performance data from a parent CC foil on data from the conventional foil. This method is useful for tests that use elliptical sections; however, when using a NACA 6-series parent section, the trailing edge differs significantly from the original pointed trailing edge. Therefore, this method is not practical for these predictions.

EXPERIMENTAL RESULTS

Results

Experimental testing shows that the design of the CC foil is effective. Span-wise flow from the trailing edge of the CC foil proves to be uniform, and the trailing edge radius is effective. Analysis of the lift and drag characteristics was performed by comparing the effect of varying flow channel speeds on the non-dimensional lift and drag coefficients.

The first set of foil testing was conducted without a lower end plate, enabling analysis of three-dimensional effects. The CC foil was tested with velocity ratios of 1, 2, 3, and 4 and compared to the conventional foil at varying angles of attack and flow channel velocities. A comparison of the lift coefficient to angle of attack for a flow channel speed of 1.8 ft/s is shown in Figure 27. The conventional foil produces less lift than does the CC foil at all angles of attack and velocity ratios. Each increase in velocity ratio results in a dramatic increase in lift coefficient. The CC foil with a velocity ratio of 4 enjoys a 30% larger lift coefficient at an angle of attack of zero degrees than does the conventional foil at an angle of attack of eight degrees.

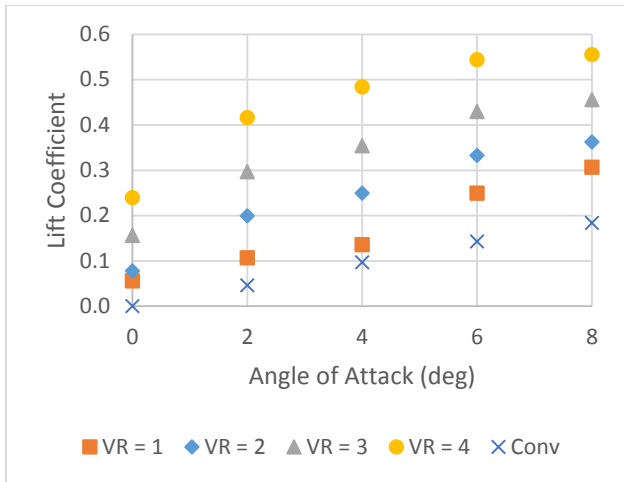


Figure 27. Lift Coefficient to Angle of Attack of 3D Foils

A similar trend is seen for the drag coefficient, with higher jet velocities producing more induced drag, resulting in higher drag coefficients. The plot of drag coefficient to angle of attack for a flow channel speed of 1.8 ft/s is shown in Figure 28. With the exception of a velocity ratio of two at an eight degree angle of attack, each increase in velocity ratio corresponded to an increase in drag over the testing spectrum. The conventional foil exhibits the least drag across the all angles of attack, as expected. The CC foil does not exhibit the same constant drag coefficient over any set of angles of attack, showing that there is no “drag bucket” on CC foils. The drag for the CC foil at an angle of two degrees may be understated because of the large uncertainty in those data points that potentially resulting from resonance of the foil.

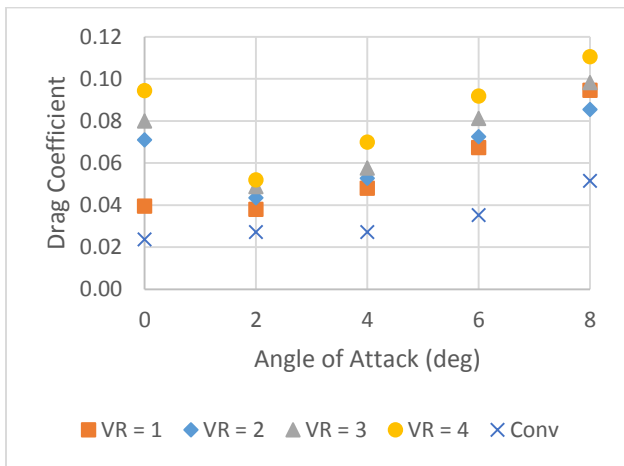


Figure 28. Drag Coefficient to Angle of Attack of 3D Foils

In determining the advantages of CC relative to a conventional foil, the lift-to-drag characteristic is a key measure of merit. A lift-to-drag comparison of the same flow channel speed is shown in Figure 29. For higher velocity ratios, the lift-to-drag characteristics of the CC foil make it beneficial when compared to the conventional foil over the spectrum of angles tested. At a velocity ratio of one, the lift-to-drag characteristics are worse than those of the conventional foil at some angles of attack. This decreased lift-to-drag is to be expected because the geometry of the CC foil has greater drag than the conventional foil, and very low velocity ratios do not take advantage of the lift-producing effects of CC. The lift-to-drag characteristics of the CC foil at an angle of attack of two degrees are likely overstated as a result of the uncertainty in the drag results, as previously mentioned.

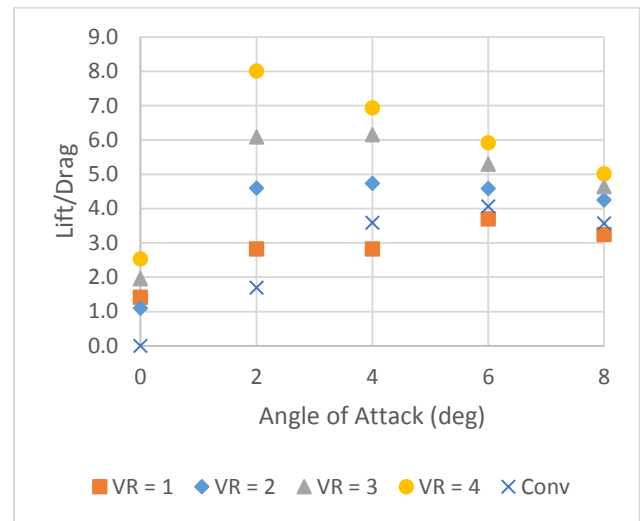


Figure 29. Lift-to-Drag Ratio to Angle of Attack of 3D Foils

A second set of 3D testing was conducted with the jet velocity held constant, while the flow channel speed was varied. A plot of the effect of flow channel speed on the lift coefficient for the finite-span CC foil is shown in Figure 30. The lift coefficient decreased as the flow channel speed was increased, which is to be expected because it shows that CC produced less lift at lower velocity ratios. Larger jet velocities result in larger lift coefficients across the range of flow channel speeds, meaning that a higher momentum coefficient consistently produces more lift at any given channel speed.

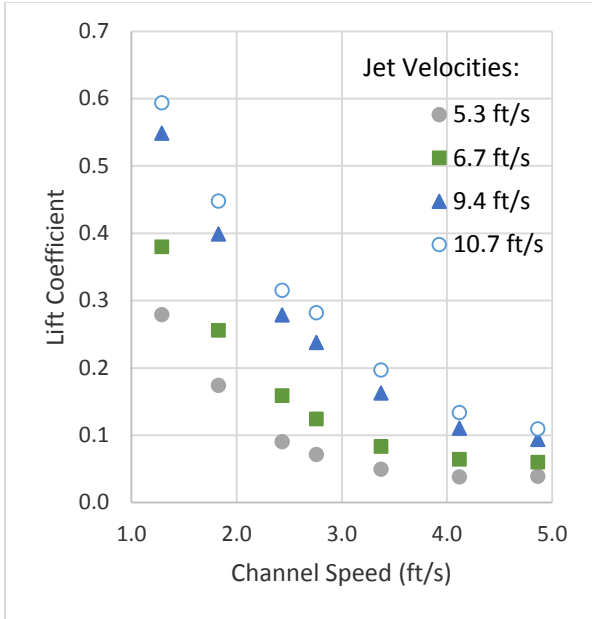


Figure 30. CC 3D Lift Coefficient to Flow Channel Speed at Zero Degrees for Different Jet Velocities

Because the drag force resulting from a CC foil is not related directly to the jet velocity, the drag coefficient is expected to be much more dependent upon the flow channel speed than the jet velocity. The drag coefficients for the finite-span foils are shown in Figure 31. The difference between drag coefficients at low speeds, where the velocity ratio was in excess of 4.0, was found to be highly dependent upon the jet velocity, with the highest jet velocities resulting in the largest drag. As flow channel speeds increased, the drag coefficients converged very quickly, showing that the geometric drag of the foil is the primary source of drag at higher speeds.

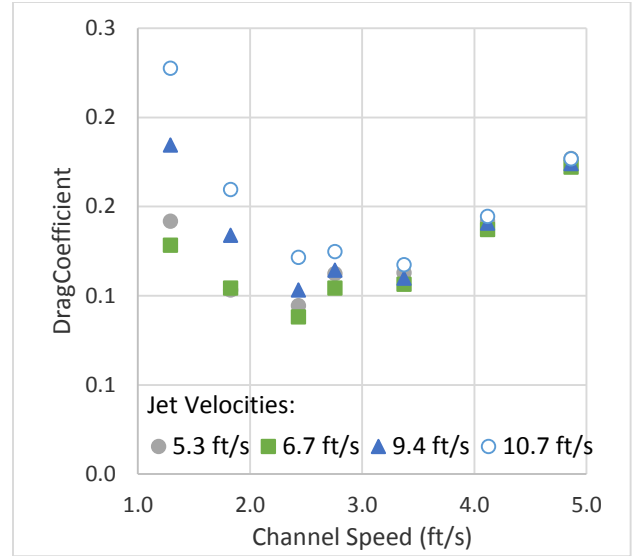


Figure 31. CC 3D Drag Coefficient to Flow Channel Speed at Zero Degrees for Different Jet Velocities

2D vs. 3D Characteristics

The CC foil was expected to exhibit similar finite-span lift losses as a conventional foil. The lift coefficients at varying angles of attack and flow channel speeds for the CC foil at a velocity ratio of 2.0 are shown in Figure 32. In all cases, the two-dimensional foil resulted in more lift at a given angle of attack than the three-dimensional foil. At higher angles of attack and higher speeds, the advantages of two-dimensional flow are magnified, as expected from conventional circulation theory.

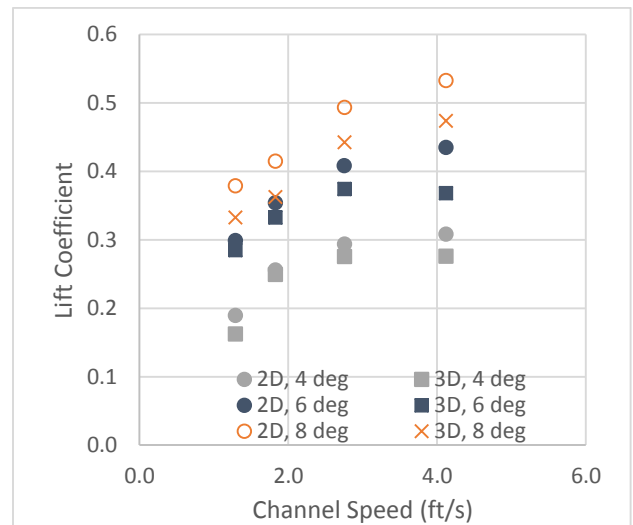


Figure 32. CC 2D vs. 3D Lift Coefficient Comparison

Using Helmbold's equation relating two-dimensional and three-dimensional lift coefficients and Ward's equation relating two-dimensional lift to the momentum coefficient, we were able to establish the results expected from 3D theory. It is apparent from Figure 33 that our 3D results fit the expected trend well. In order to fit this trend, however, Ward's equation must be modified. Ward's equation represents the lift coefficient as a function of the square-root of the momentum coefficient multiplied by a constant. In order for our results to be comparable to theory, the constant had to be reduced by 20%. It is apparent that Helmbold's equation, which was originally intended for conventional foils, can be applied to CC foils.

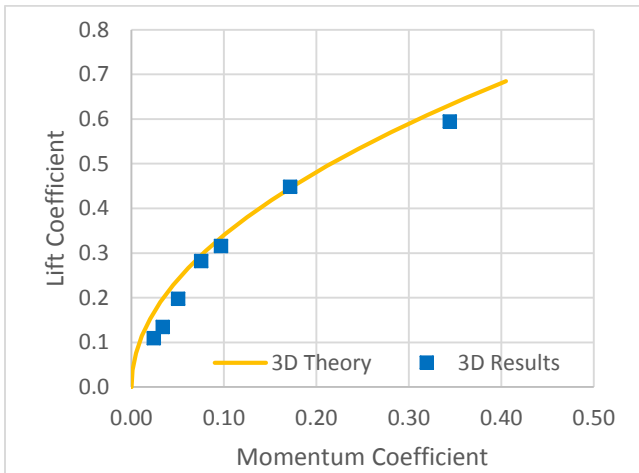


Figure 33. 3D Theory Comparison

Zero Jet Velocity Characteristics

Although the comparison of the CC and conventional foils in their operating ranges determines when it will be advantageous to use CC, it does not determine the performance changes arising solely from changes in foil geometry. Testing was completed at zero jet velocity, allowing the comparison of the two foil geometries. It was expected that the CC foil at zero jet velocity would produce less lift and more drag than the conventional NACA foil. In this analysis, the lift-to-drag characteristics, shown in Figure 34, are of key importance. The CC foil exhibited characteristics that were significantly worse than the conventional foil, with increasing angle of attack resulting in an increasing discrepancy. Therefore, it is apparent that the advantages of applying CC are not a result of the difference in geometry, but rather the

CC geometry has detrimental effects in the zero jet velocity condition.

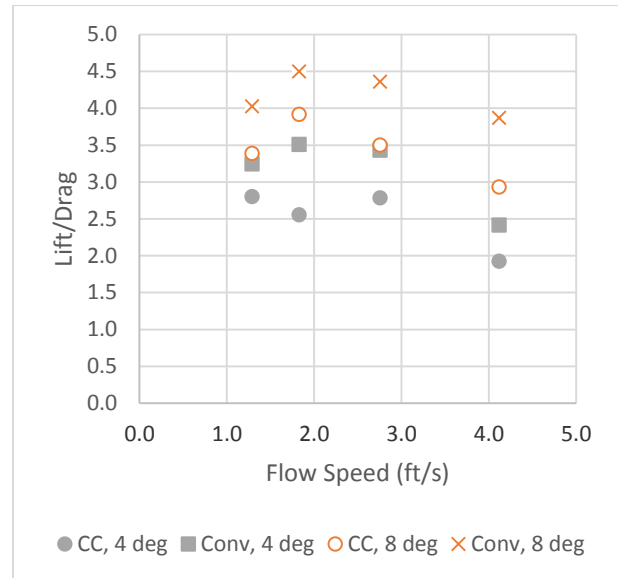


Figure 34. Zero Jet Velocity Comparison

Uncertainty

Flow channel testing data contains natural uncertainty resulting from the testing equipment. In order to determine the magnitude of this uncertainty, an analysis was performed on the calibration data. The calibration data, which were collected before and after each set of testing, were analyzed by dividing their standard deviation by the square root of the number of calibration points. This value was then taken as a percentage uncertainty, which was found to be less than 1% for drag and less than 5% for lift.

Sources of Error

With the CC foil attached to the apparatus, a harmonic response at flow speeds between 1.8 and 2.4 ft/s, corresponding to motor frequencies of 6 to 8 Hertz was seen. The conventional foil experienced some resonance at 10 Hertz, corresponding to a flow velocity of approximately 3 ft/s, but the amplitude was significantly smaller.

Motor frequencies of 18 Hertz or higher, corresponding to flow velocities greater than 4.9 ft/s, created some cavitation resulting in bubbles in the flow. These bubbles occur because of abrupt changes in channel geometry. Bubbles flowing along the foil potentially affected the pressure field.

The Hydronix flow meters that were used to measure the jet velocity have an accuracy of $\pm 5\%$ according to the manufacturer cut sheet. Additionally, the stereolithography tolerance in the direction of the slot height is ± 0.002 inch, which introduces an additional 5% of inaccuracy. These combined inaccuracies could result in a total jet velocity discrepancy of up to 10%.

There was drift in the gain and bias of the force blocks during each set of tests. The drift in the bias has negligible effect on the results, because a zero was recorded prior to each test. Recording zeroes periodically allowed for the data to be zeroed to a calm water condition at multiple points throughout each session of testing. The drift in the gain, however, could not be mitigated during testing in the same manner. The maximum drift recorded over the entire set of tests was 3.3%.

CONCLUSION

The results demonstrate that the CC foil was designed properly to produce increased lift at non-zero angles of attack and to generate lift even at an angle of attack of zero. The span-wise uniform jet flow shows that applying the Bernoulli equation along the length of the plenum is effective and eliminates the use of screens that have been used to regulate flow in previous experiments.

The results show that an increasing velocity ratio results in a dramatic increase in lift, but with only a small increase in drag. Analysis of the drag characteristics shows that at low speeds the jet momentum produces high drag, but at higher speeds the drag arising from the foil geometry becomes more critical. The lift-to-drag ratio shows that with velocity ratios above 2.0, the application of CC is beneficial; however, at lower velocity ratios there is a point where the conventional foil is more advantageous as the lift-to-drag ratio overtakes that of the CC foil. Conventional three-dimensional theory, particularly Helmholtz's equation, is seen to be applicable to CC foils based on this analysis.

The CC foil's lift and drag characteristics are comparable to previous work on CC and show that modern foils can be modified for use with CC. There is potential for CC to be applied to marine control

surfaces in order to increase lift on conventional surfaces or to eliminate the need for changing angles of attack.

RECOMMENDATIONS FOR FUTURE WORK

There is significant experimental data for CC wings of high-aspect ratios. This thesis and the work of Rogers and Donnelly (2004) provide useful data for the validation of a viscous flow computational fluid dynamics (CFD) code for wings with aspect ratios less than two. The purpose of this CFD analysis is to guide future design of trailing edge details involved in a CC wing. Some parameters that must be considered include: trailing edge radius, slot height, jet velocity, and possible use of methods to encourage flow detachment along the trailing edge radius. It would also be useful to investigate the effect of thickness ratio and camber of a CC wing.

In addition to validating CFD, additional experimental work will be useful to future design. A line of pressure taps can be placed around a CC section to confirm the chord-wise pressure distribution that was assumed in the initial predictions prior to the experimental work completed in this thesis. This would also be useful for comparison with inviscid panel-method pressure-distribution data from previous work. Particle image velocimetry could be applied for flow visualization. Flow visualization is useful to determine the angle around the trailing edge at which the flow separates from the radius at different momentum coefficients and angles of attack.

There have been numerous experimental proofs-of-concept for CC applications performed at model scale. Full-scale experimental testing is necessary prior to any commercial implementation of this technology. There currently is no consensus regarding the effects of Reynolds number for CC lift. A change in Reynolds number can cause a shift in the flow separation point. There is potential for flow separation prior to the slot. For a thesis at Webb Institute, a full-scale application is likely unfeasible. There is potential for further CFD work related this issue.

Additional means of controlling circulation around a surface exist for increasing lift. A similar foil could be constructed that replaces the rounded trailing edge and slot used in this thesis with a rotating trailing edge. The rotation of the trailing edge will take advantage of the Magnus effect, allowing the wake sheet to be deflected similar to a CC foil wake sheet. It would be interesting to compare the power required to operate the pump used in this thesis with the power required by a motor to rotate the trailing edge a Magnus effect foil producing the same force as a CC foil.

REFERENCES

- Abbott, Ira H., and Albert E. von Doenhoff. 1949. *Theory of Wing Sections*. New York: Dover Publications, Inc.
- Anderson, John D. 2014. "Airfoil." *McGraw-Hill Education*.
<http://www.accessscience.com/content/airfoil/019500>.
- Brown, Neal A. 2000. *Coanda Circulation Control Maneuvering System*. New Orleans: Gulf Coast Region Maritime Technology Center.
- Day, Terry. 2008. "The Coanda Effect and Lift." *New Fluid Technology*.
www.newfluidtechnology.com.
- Englar, R. J. 2004. "Experimental Development and Evaluation of Pneumatic Powered-Lift Super-STOL Aircraft." *Proceedings of the 2004 NASA/ONR Circulation Control Workshop*. Hampton: NASA/ONR. 577-602.
- Englar, Robert J. 1975. *Experimental Investigation of the High Velocity Coanda Wall Jet Applied to Bluff Trailing Edge Circulation Control Airfoils*. Bethesda: David W. Taylor Naval Ship Research and Development Center.
- Englar, Robert J., and Robert M. Williams. 1971. *Design of a Circulation Control Stern Plane for Submarine Applications*. Bethesda: Naval Ship Research and Development Center.
- Imber, Robin. 2004. "Exploratory Investigations of Circulation Control Technology: Overview for Period 1987-2003 at NSWCCD." *Proceedings of the 2004 NASA/ONR Circulation Control Workshop*. Hampton: NASA/ONR. 577-602.
- Kweder, Jonathan, Chad C. Panther, and James E. Smith. 2010. "Applications of Circulation Control, Yesterday and Today." *International Journal of Engineering* 411-29.
- Kweder, Jonathan, Zachary J. Luzader, Michael J. Spencer, Andrew D. Lowery, and James E. Smith. 2012. "The Development and Experimental Testing of a Lift Augmented Propeller." *International Journal of Engineering and Innovative Technology* 125-34.
- Larsson, Lars, and Rolf E. Eliasson. 2007. *Principles of Yacht Design*. Camden, Maine: McGraw-Hill.
- MD Helicopters. 2013. November 16. http://mdhelicopters.com/img/About_1.jpg.
- Munson, Bruce R., Donald F. Young, and Theodore H. Okiishi. 2006. *Fundamentals of Fluid Mechanics*. Hoboken: John Wiley & Sons.
- Rogers, Ernest O., and Martin J. Donnelly. 2004. *Characteristics of a Dual-Slotted Circulation Control Wing of Low Aspect Ratio Intended for Naval Hydrodynamic Applications*. West Bethesda: Naval Surface Warfare Center.
- Ward, Craig Christopher. 2006. *Circulation Control Technique on a Marine Propeller Duct*. Glasgow: Universities of Glasgow and Strathclyde.
- Zhu, Songlin. 1996. *Research and Development of a High Lift Rudder*. Chapel Hill: University of North Carolina.

ACKNOWLEDGMENTS

The successful completion of this thesis could not have been possible without the help of the professors and technicians at Webb Institute. We would like to thank our principal advisor, Professor Royce, for his guidance and help at every stage of both iterations of this thesis. Additionally, we would like to thank Professor Gallagher, Pat Doherty and Jamie Swan for their help preparing Robinson Model Basin and the circulating water channel for our use.

Samuel M. Granger completed his bachelors degree at Webb Institute in June of 2014 and is now a naval architect at Glosten in Seattle, WA.

Randall P. Neureuter completed his bachelors degree at Webb Institute in June of 2014 and is now a naval architect at Guido Perla & Associates, Inc. in Seattle, WA.